EuroIntervention 2019;15:919-922

Dynamic anatomic relationship of the coronary arteries to the valves. Part 1: mitral annulus and circumflex artery

Ricarda Hinzpeter[1]*, MD; Matthias Eberhard[1], MD; Alberto Pozzoli[2], MD; Jochen von Spiczak[1], MD, Msc; Robert Manka[1,3,4], MD; Felix C. Tanner[3], MD; Maurizio Taramasso[2], MD; Francesco Maisano[2], MD; Hatem Alkadhi[1], MD, MPH, EBCR, FESER

1. Institute of Diagnostic and Interventional Radiology, University Hospital Zurich, University of Zurich, Zurich, Switzerland; 2. Department of Cardiovascular Surgery, University Hospital Zurich, University of Zurich, Zurich, Switzerland; 3. Department of Cardiology, University Heart Center Zurich, University of Zurich, Zurich, Switzerland; 4. Institute for Biomedical Engineering, University and ETH Zurich, Zurich, Switzerland

This paper also includes supplementary data published online at: https://eurointervention.pcronline.com/doi/10.4244/EIJ-D-19-00669

Introduction

Mitral regurgitation (MR) represents one of the most common valvular heart diseases affecting almost 10% of the population >75 years of age[1]. According to the American College of Cardiology/American Heart Association, surgical interventions still represent the gold standard for treatment of severe MR[2]. However, many patients do not undergo surgery due to increased surgical risk, which has driven the field of percutaneous mitral valve (MV) treatments, including repair and replacement technologies[3]. As catheter-based MV repair options are increasingly adopted in clinical practice, they require accurate preprocedural imaging, providing detailed anatomic information about the MV and adjacent structures such as the circumflex artery (Cx) to avoid periprocedural injury[1].

This study comprehensively assessed the dynamic anatomic relationship between the mitral annulus (MA) and Cx in normal subjects and in patients with severe MR.

Methods

Twenty patients with severe primary MR, determined by transthoracic echocardiography, termed "patients", and 20 patients without cardiac disease, termed "controls", undergoing computed tomography (CT) were included **(Table 1)**. All subjects had right dominant coronary supply.

CT DATA ANALYSIS

Image analysis was performed using a prototype advanced visualisation, segmentation and image analysis software (3mensio Structural Heart 6.0 beta; Pie Medical Imaging, Maastricht, the Netherlands). MA and Cx dimensions, and distances between the MA and Cx were measured in all phases by two independent readers **(Figure 1)**.

Details regarding CT protocol and statistical analysis can be found in **Supplementary Appendix 1** and **Supplementary Appendix 2**.

Results

DIMENSIONS AND GEOMETRY OF THE MA AND CX

MA areas and circumferences were significantly larger, and the Cx was significantly longer in patients than in controls in all phases ($p<0.001$) **(Table 1, Supplementary Table 1)**. The MA showed no increased flattening (difference between three-dimensional [3D]

**Corresponding author: Institute of Diagnostic and Interventional Radiology, University Hospital Zurich, Raemistr. 100, CH-8091 Zurich, Switzerland. E-mail: ricarda.hinzpeter@usz.ch*

SUBMITTED ON 19/07/2019 - REVISION RECEIVED ON 29/08/2019 - ACCEPTED ON 10/09/2019

DOI: 10.4244/EIJ-D-19-00669

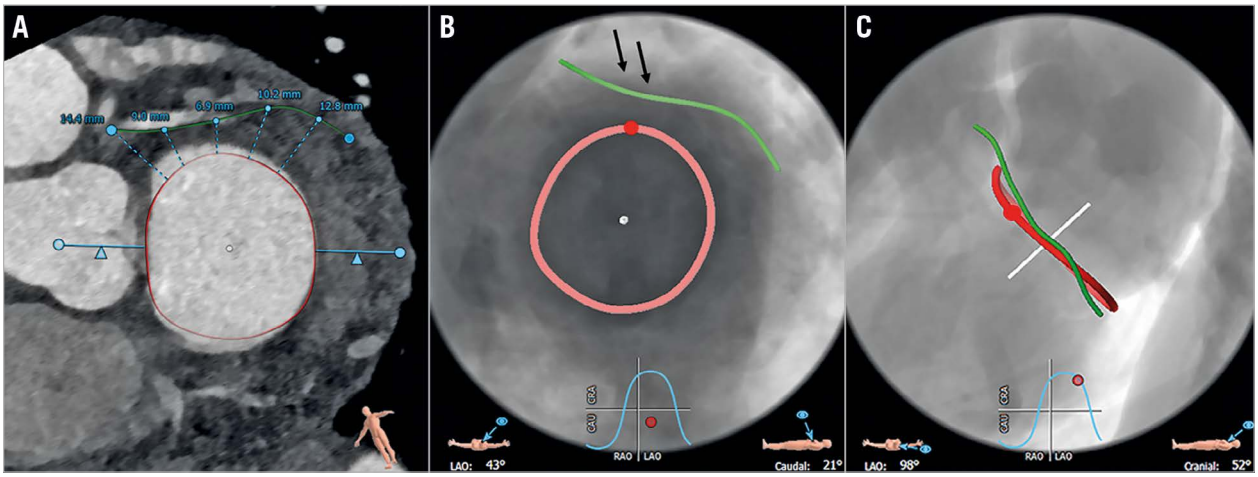

Figure 1. *Image analysis. CT (A) and fluoroscopic views of the MA and Cx in a patient with severe MR (B: 43° LAO; C: 98° LAO) in mid-diastole (80%), including distance measurements of five seed points in this representative patient (average number of seed points, n=6) (A). Black arrows: short segment of the proximal Cx with consistently narrowest distances (B), opposite the ALC (indicated by red point).*

Table 1. Demographics (mean±SD).

		Patients	Controls	*p*-value
Number of patients		20	20	
Age (years)		63±11	68±9	0.22
Sex	Male	16 (80%)	17 (85%)	0.68
	Female	4 (20%)	3 (15%)	
Body mass index (kg/cm^2)		27±5	29±5	0.33
Left ventricular ejection fraction (%)		59±13	60±9	0.86
Heart rate during CT (bpm)		86±22	65±8	0.001
Cx length (mm)		59.3±11.1	52.7±7.0	0.03
Annular circumference - systole (mm)		130.3±18.6	106.2±6.9	<0.001
Annular circumference - diastole (mm)		129.9±14.5	108.2±4.5	<0.001
Annular area - systole (cm^2)		12.6±3.4	8.2±1.1	<0.001
Annular area - diastole (cm^2)		12.7±2.7	8.6±0.7	<0.001

SD: standard deviation

and two-dimensional [2D]) in patients compared to controls, but 3D geometry of the MA was maintained in both groups (difference between 3D and 2D: 2.8 mm in patients; 2.6 mm in controls).

DISTANCES AND SPATIAL RELATIONSHIP OF THE MA TO THE CX

Distances between the MA and Cx were significantly larger in patients compared to controls for all measurement points and all phases (p=0.001-0.008) **(Figure 2)**. In both cohorts, distances between the MA and Cx continuously decreased until point 3 and increased to the last point.

The shortest distances between the MA and Cx were found in patients in the proximal segment in mid-systole (30%) and in controls in the proximal segment in early systole (10%) **(Table 2)**.

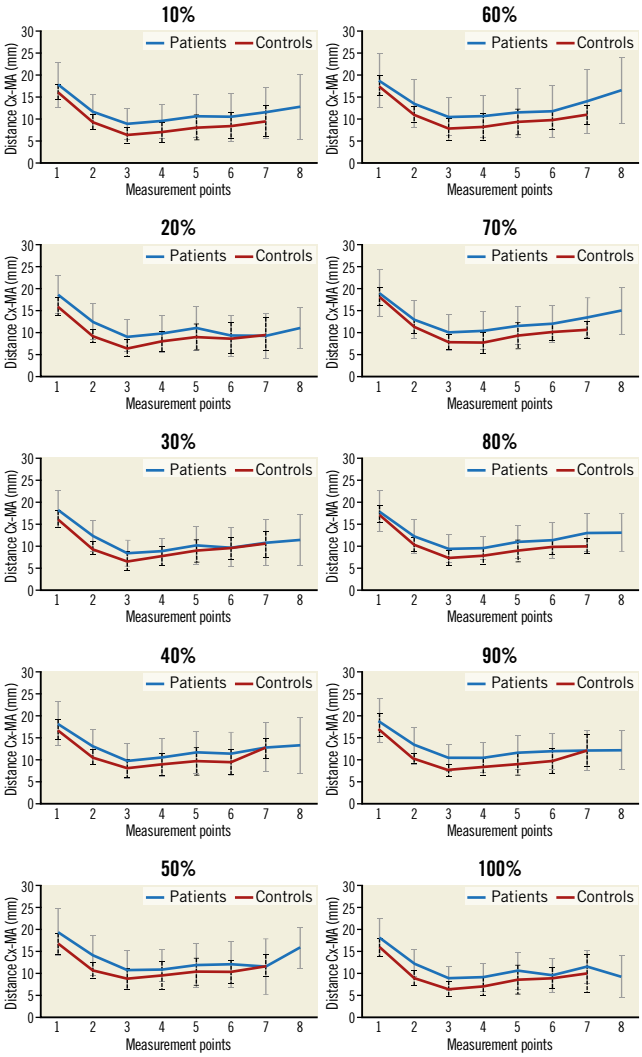

Figure 2. *Distances (and SD) between the Cx and MA for all measurements and phases in patients with severe MR (blue line; SD: grey line) and controls (red line; SD: black dashed line).*

Table 2. Distances between the MA and Cx for all measurements and all phases in both groups. Coloured boxes indicate shortest distances. Dark red: shortest overall distance; light red boxes: <9 mm; orange: 9-10 mm; yellow: 10-12 mm; light yellow: >12 mm.

Patients	1	2	3	4	5	6	7	8
10%	17.66	11.61	8.91	9.47	10.56	10.34	11.40	12.74
20%	18.61	12.46	9.14	9.74	10.95	9.23	9.12	10.92
30%	18.58	12.53	8.59	8.98	10.27	9.89	10.93	11.62
40%	18.24	12.85	9.67	10.38	11.58	11.29	12.74	13.19
50%	19.34	14.08	10.72	10.81	11.85	12.01	11.50	15.89
60%	18.81	13.46	10.43	10.50	11.39	11.66	13.96	16.48
70%	18.95	12.96	9.94	10.31	11.43	11.84	13.34	14.85
80%	18.21	12.36	9.61	9.81	11.07	11.41	13.19	13.22
90%	18.81	13.38	10.34	10.42	11.47	11.89	12.00	12.14
100%	18.20	12.32	8.77	9.11	10.45	9.51	11.36	9.13
Controls	**1**	**2**	**3**	**4**	**5**	**6**	**7**	**8**
10%	16.11	9.24	6.22	6.93	8.01	8.49	9.50	–
20%	15.92	9.12	6.49	7.88	8.92	8.63	9.54	–
30%	16.31	9.74	6.73	7.88	9.04	9.65	10.56	–
40%	16.83	10.49	8.00	8.86	9.61	9.36	12.55	–
50%	16.71	10.59	8.72	9.48	10.37	10.27	11.73	–
60%	17.51	10.98	7.73	8.12	9.27	9.69	10.90	–
70%	18.17	11.33	7.75	7.57	9.18	10.05	10.53	–
80%	17.46	10.56	7.49	7.95	9.04	9.96	10.14	–
90%	16.99	10.21	7.56	8.32	8.92	9.60	12.07	–
100%	15.88	8.87	6.47	7.04	8.55	8.89	9.99	–

In both cohorts and in all phases the anterolateral commissure (ALC) was opposite to measurement points 3 and 4 (proximal Cx) **(Figure 1)**.

Displacement of the Cx in relation to the MA throughout phases compared between mid-systole (30%) and mid-diastole (70%) was similar in the proximal Cx (measurement point 3) for both groups, whereas larger displacements were found in patients in distal Cx segments in systole **(Supplementary Figure 1)**.

Discussion

We consistently found larger areas and circumferences of the MA and a longer Cx in patients than in controls. There was a consistent relationship between the Cx and MA throughout the cardiac cycle, showing overall larger distances in patients compared to controls, with decreasing distances between the Cx and the MA to the level of the ALC, while distances progressively increased more distally.

Our study revealed 3D distances between the Cx and MA of between 6.2±1.9 and 6.9±2.4 mm in controls and 8.6±2.9 and 9.0±3.0 mm in patients, including overall shortest distances in the proximal segment in both groups (controls: 6.2±1.9 mm; patients: 8.6±2.9 mm).

Our analyses confirm previous results[3] comparing distances between the MA and Cx in controls and in patients with left ventricular (LV) dysfunction and/or MR, measuring larger distances in patients compared to controls (7.6±2.3 mm vs 5.8±1.8 mm), with shortest distances in the proximal to mid Cx (average 6.4±2.1 mm). The ALC corresponds to the origin of the P1 segment of the posterior leaflet. Thus, caution must be exercised to avoid Cx injuries, as this region is the landmark for anchor positioning of most direct annuloplasty devices.

Cardiac motion is larger at the base of the heart at the location of the atrioventricular groove than anteriorly in the course of the left anterior descending (LAD) artery. Similar to the right coronary artery (RCA), the Cx shows large displacement with highest movements in systole[4,5]. Consistent with that, we found a higher displacement of the Cx in systole, being more pronounced for mid and distal Cx segments, with reduction of displacement at end-systole in the proximal Cx.

Limitations

The retrospective study design, small number of patients (none with left coronary dominance) and the fact that the study was not designed for a specific device are all limitations.

Conclusion

Our study includes a detailed analysis of the 3D dynamics between the MA and Cx throughout the cardiac cycle in controls and patients with severe MR. In patients, the shortest distances between the MA and Cx were found in mid-systole in the proximal Cx, opposite the ALC, which is an important landmark for annuloplasty devices.

Impact on daily practice

Transcatheter therapies for MR require pre-interventional imaging to obtain detailed and comprehensive knowledge of the MV geometry and its relationship to adjacent structures such as the Cx to avoid potentially fatal injury.

Conflict of interest statement

M. Taramasso is a consultant for St. Jude Medical, and also reports personal fees from Abbott Vascular, Boston Scientific, 4Tech, Edwards Lifesciences and CoreMedic, outside the submitted work. F. Maisano is a co-founder of 4Tech, a consultant for Abbott Vascular, St. Jude Medical, Medtronic and Valtech Cardio, receives royalties from Edwards Lifesciences, and also reports personal fees from Abbott, Edwards Lifesciences, Mitraltech, and other from Edwards Lifesciences, Mitraltech and 4Tech, outside the submitted work. The other authors have no conflicts of interest to declare.

References

1. Naoum C, Blanke P, Cavalcante JL, Leipsic J. Cardiac Computed Tomography and Magnetic Resonance Imaging in the Evaluation of Mitral and Tricuspid Valve Disease: Implications for Transcatheter Interventions. *Circ Cardiovasc Imaging*. 2017;10:e005331.

2. Zamorano JL, Gonzalez-Gomez A, Lancellotti P. Mitral valve anatomy: implications for transcatheter mitral valve interventions. *EuroIntervention*. 2014;10:U106-11.

3. Ghersin N, Abadi S, Sabbag A, Lamash Y, Anderson RH, Wolfson H, Lessick J. The three-dimensional geometric relationship between the mitral valvar annulus and the coronary arteries as seen from the perspective of the cardiac surgeon using cardiac computed tomography. *Eur J Cardiothorac Surg*. 2013;44:1123-30.

4. Vembar M, Garcia M, Heuscher DJ, Haberl R, Matthews D, Böhme GE, Greenberg NL. A dynamic approach to identifying desired physiological phases for cardiac imaging using multislice spiral CT. *Med Phys*. 2003;30:1683-93.

5. Sundermann SH, Gordic S, Manka R, Cesarovic N, Falk V, Maisano F, Alkadhi H. Computed tomography for planning and postoperative imaging of transvenous mitral annuloplasty: first experience in an animal model. *Int J Cardiovasc Imaging*. 2015;31:135-42.

Supplementary data

Supplementary Appendix 1. Methods.

Supplementary Appendix 2. Results.

Supplementary Figure 1. Displacement of the circumflex artery in relation to the mitral annulus in one cardiac cycle.

Supplementary Table 1. 2D and 3D dimensions of the MA in each phase of the cardiac cycle.

The supplementary data are published online at: https://eurointervention.pcronline.com/doi/10.4244/EIJ-D-19-00669

Supplementary data

Supplementary Appendix 1. Methods

CT data acquisition and image reconstruction

CT examinations were performed on a first- (n=7, SOMATOM Definition; Siemens Healthineers, Forchheim, Germany), second- (n=5, SOMATOM Flash; Siemens) or third-generation dual-source CT scanner (n=8, SOMATOM Force; Siemens). The scan range covered the entire heart in a cranio-caudal direction. All subjects were in sinus rhythm; no β-blockers were administered prior to CT.

A standardised, weight-adapted contrast media protocol was used administering 60-80 ml of pre-warmed non-ionic, iodinated contrast media (Iopromidum, Ultravist 370, 370 mg/ml; Bayer Schering, Berlin, Germany) through an antecubital vein with a flow rate of 5-6 ml/s followed by the same volume consisting of 20% contrast media and 80% saline solution. Contrast agent application was controlled by bolus tracking in the ascending aorta (attenuation threshold 120 HU at 120 kVp). CT data acquisition was performed using standard protocol settings and with a spiral data acquisition mode synchronised to the electrocardiogram (ECG) in a retrospective mode using ECG pulsing from 30-80% of the RR interval. The average $CTDI_{vol}$ of the protocol was 482±18 mGy. In each patient and control, a total of 10 data sets were reconstructed throughout the cardiac cycle in 10% steps from 10-100% of the RR interval.

CT data analysis

After manually placing 16 seed points along the hinge points of the MA (in the long-axis reformation) in each data set, the circumference and the area of the MA were automatically determined. Subsequently, the Cx was defined by placing seed points along the margin of the vessel facing the MA from the bifurcation or trifurcation of the left main artery (LM). Seed points were placed until the Cx branched off, the posterior atrioventricular groove eventually giving rise to a posterolateral branch. By placing one marker at the origin of the Cx and one at the termination of the vessel in the posterior atrioventricular groove, the length of the vessel was automatically determined. The shortest distances in the 3D space from the MA to the Cx were generated semi-automatically in 1 cm distances along the Cx based on the previously defined MA (average number of seed points in controls and in patients with severe MR: n=6; **Figure 1**).

Definition of measurements

In addition to the shortest 3D distances from the MA to the Cx at each seed point, the following measurements of the mitral valve complex were made:

Area: the annular surface area with projection of the annulus to a plane perpendicular to the mathematical centre of the mitral annulus.

Entire MA circumference 3D: the length of the entire mitral annular circumference in 3D.
Entire MA circumference 2D: the length of the entire mitral annular circumference in 3D projected to a 2D plane perpendicular to the mathematical centre.

Cx: the length of the Cx from the bifurcation or trifurcation of the LM to the origin of the posterolateral branch determining the termination of the Cx.

Statistical analysis

Quantitative variables were expressed as means±standard deviations for normally distributed values. Ordinal variables were expressed as frequencies and percentages. Normality was tested using the Shapiro-Wilk test. The χ^2 test was used for differences between groups regarding gender. The Mann-Whitney U test was used for differences between groups regarding age, body mass index (BMI in kg/cm^2), LVEF (in %), heart rate during CT, the length of the Cx, and the geometric measurements of the MA. Differences between groups regarding distances of the MA to the Cx were calculated using the Wilcoxon signed-rank test. To determine the inter-observer agreement between the two readers, the intraclass correlation coefficient (ICC) was calculated. According to Landis and Koch, ICC values of 0.61-0.80 were interpreted as substantial and 0.81-1.00 as excellent agreement. Additionally, Bland-Altman analysis was performed to assess agreement between the two readers. Data were analysed using commercially available software, SPSS Statistics, Version 25.0 (IBM Corp., Armonk, NY, USA). A two-tailed p-value <0.05 was considered statistically significant.

Supplementary Appendix 2. Results

Interreader agreement

The interreader agreement between the two readers was excellent for all measurements of the MA (area in all phases: ICC 0.84-0.99; 2D annular circumference in all phases: ICC 0.82-0.99; 3D annular circumference in all phases: 0.81-0.99). Similarly, measurements of the 3D distances from the MA to the Cx in all phases from every seed point showed excellent agreement between readers both in controls and in patients with severe MR (ICC: 0.98-1.00). Because of the excellent interreader agreement, average values from both readers were used for further data analysis. Bland-Altman analyses revealed minimal errors between readers for all measurements in mid-systole (at 30%) and mid-diastole (at 70%) (area: mean difference -0.2±0.7; 95% CI: -1.94-1.21; 2D and 3D annular circumference -2.2±4.6- and -0.7±3.2; 95% CI: -8.61-6.94; distances from the TA to the RCA -0.02±1.1 and -0.5±1.0; 95% CI: -2.21-1.95).

Supplementary Figure 1. Displacement of the circumflex artery to the mitral annulus.

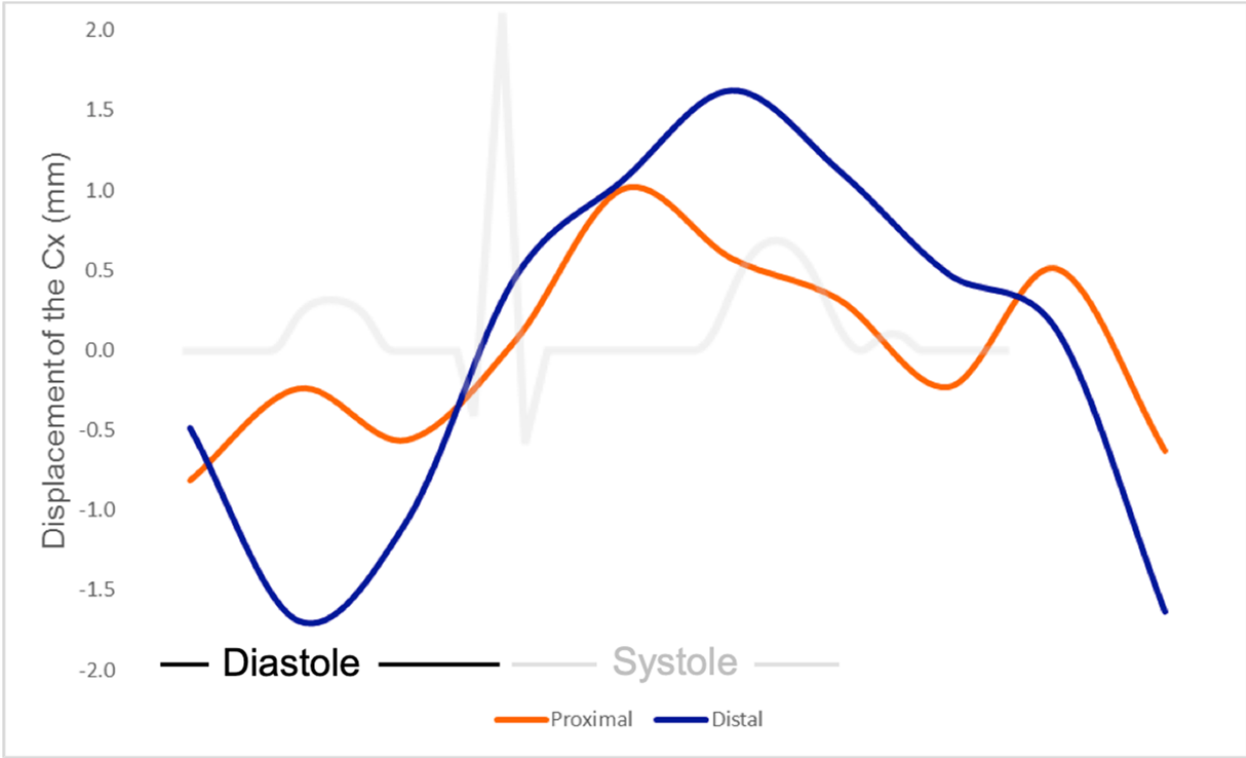

Displacement of the Cx in relation to the MA in one cardiac cycle in patients with severe MR, displayed for the proximal (orange line, mean values of measurement points 1-3) and distal (blue line, mean values of measurement points 4-6) segments separately. The amplitude indicates the extent of movement between the Cx and MA, with positive values indicating motion of the Cx towards the MA. Note maximum displacement of the Cx in the distal segment in mid-systole and mid-diastole.

Supplementary Table 1. 2D and 3D dimensions of the MA in each phase of the cardiac cycle.

	10%	20%	30%	40%	50%	60%	70%	80%	90%	100%
Controls										
Annular area (cm^2)	8.6	8.6	8.6	8.2	8.4	8.6	8.5	8.6	9.1	8.4
3D perimeter (mm)	109.8	109.4	108.6	106.2	106.2	107.4	107.4	108.2	111.1	108.4
2D perimeter (mm)	106.8	106.9	106.0	103.6	104.4	105.8	105.8	106.9	109.2	105.8
Patients with severe MR										
Annular area (cm^2)	12.7	13.1	13.1	12.6	12.4	12.8	12.6	12.7	13.0	12.5
3D perimeter (mm)	130.4	131.4	131.9	130.3	127.5	128.8	129.1	129.9	130.8	129.3
2D perimeter (mm)	127.5	128.8	129.7	126.8	125.3	126.5	124.4	127.8	128.7	126.8